Population dynamics of driven autocatalytic reactive mixtures

Hongbo Zhao[1] and Martin Z. Bazant[1,2]

[1]*Department of Chemical Engineering, Massachusetts Institute of Technology, 25 Ames Street, Cambridge, Massachusetts 02139, USA*

[2]*Department of Mathematics, Massachusetts Institute of Technology, 77 Massachusetts Avenue, Cambridge, Massachusetts 02139, USA*

(Received 4 February 2019; published 26 July 2019)

Motivated by the effect of electroautocatalysis (explicit concentration dependence) on the stability of electrochemically driven phase-separating single particles, we apply the Fokker-Planck equation to describe the population dynamics of a general ensemble of chemically reactive particles. For phase-separating ensembles, we show that mosaic instability (from a homogeneous initial state to a multimodal probability distribution) may be suppressed or enhanced by autoinhibitory or autocatalytic reactions, respectively. In some cases, autocatalysis may induce two distinct populations in thermodynamically stable single-phase ensembles. Asymmetric reaction kinetics also results in qualitatively different population dynamics upon reversing the reaction direction. In the limit of negligible fluctuations, we use the method of characteristics and linearization to study the evolution of the concentration variance as well as the condition for mosaic instability, in good agreement with the full numerical solution. Applications include Li-ion batteries characterized by *in situ* x-ray diffraction.

DOI: 10.1103/PhysRevE.100.012144

I. INTRODUCTION

Population dynamics has been studied widely in particulate systems, such as crystallization, aerosol dynamics, emulsion, cell culture, etc. [1,2]. A common feature of many of these systems is the existence of intrinsic instability, either thermodynamic or kinetic in origin, that drives the evolution of the probability distribution. Examples of thermodynamic instability include Ostwald ripening [3], bistable systems such as certain Li-ion battery materials and interconnected rubber balloons [4,5], and viscoelastic crystal lattice models of plasticity [6], where population dynamics can be described by a probability distribution, e.g., in terms of a droplet or balloon size, or the lithium fraction. Examples of kinetic instability in population dynamics include autocatalytic cell growth [7], bistable gene regulatory processes [8], and CO oxidation [9–12], where coupled microelectrodes are activated sequentially upon current ramping due to negative differential resistance.

Our work is motivated by recent predictions of the control of thermodynamic instabilities by nonlinearities in the reaction kinetics, especially electroautocatalysis in driven electrochemical systems [13]. The autocatalytic effects come from an explicitly concentration-dependent prefactor on the reaction rate, which results from collective effects on the transition state of the reaction in concentrated solutions and solids [14]. In contrast, prior analyses of stochastic population dynamics using the Fokker-Planck equation, pioneered by Dreyer and co-workers [15–17] for battery materials, assume that the reaction rate is linearly proportional to the driving force, in which case the Duhem-Jougeut theorem states that thermodynamic stability is unaffected by reactions [13].

When driven far from equilibrium, the kinetic stability landscape of the system can be altered by an autocatalytic reaction kinetics, showing the suppression of thermodynamic instability in one direction and enhancement in the other, or the creation of instability in thermodynamically stable systems. This is validated in single-particle imaging experiments of lithium iron phosphate (LFP) [18,19], where lithium extraction results in a higher level of concentration heterogeneity than lithium insertion. In addition, asymmetry between the charge and discharge dynamics of lithium ion batteries is also observed in chronoamperometric experiments [20], which cannot be described by a symmetric linear kinetics. Implicit in the discussion of a concentration-dependent prefactor is that the species concentration, hence the stability, depends on the extent of reaction. This is related to, but distinct from, other state-dependent kinetics, such as velocity-dependent or space-dependent chemotaxis and van der Pol oscillation [21], as well as temporally and spatially dependent friction in activated rate processes [22–27].

In addition to instability, another aspect of interest is the collective behavior in population dynamics. Herrmann *et al.* [28,29] studied a phase transition based on Dreyer's model in the case of constant total current. The coupling of particles through the constraint of total current gives rise to a variety of regimes ranging from the Kramers-type transition and oscillatory bimodal distribution to the unimodal distribution with increasing total current. Other examples of emergent behavior have also been observed through a nonlocal interaction via moments of distribution [30] or globally coupling mean field parameters such as those in the synchronization of Kuramoto coupled oscillators [31]. Concerted behaviors observed in crowd and biological synchrony [32,33] and recently electrochemical oscillations in Li-ion batteries [34] motivate further theoretical modeling.

The population dynamics of phase-separating electrochemical systems such as LFP and graphite has also been studied through discrete particle simulations, described by multiphase porous electrode theory (MPET) [35–38]. Multiphase porous electrode theory simulates particles of random sizes in a porous electrode and resolves the spatial dependence

including the phase separation within the particles through the Allen-Cahn or Cahn-Hilliard reaction model [14]. The model also incorporates ion transport in the electrolyte. For phase-separating materials, at low current, particles are filled stochastically in a mosaic pattern. The results of the MPET model have been validated experimentally in a direct observation of lithium concentration in an ensemble of LFP nanoparticles [18]. Statistical models have also been applied to explain the chronoamperometric response [20] and scanning transmission x-ray microscopy images [39] of LFP electrodes. However, the population is categorized into untransformed, active, and transformed particles, instead of a continuous probability distribution in terms of the lithium fraction. Multiphase porous electrode theory includes all relevant physics and has shown predictive power in realistic systems but lacks an accurate statistical description as it is limited by the number of particles used in the simulation. Our theory eliminates any spatial dependence and is capable of solving for the probability distribution directly in the reaction-controlled limit.

In Sec. II we begin by connecting single-particle dynamics with population dynamics through the concept of autocatalysis in Sec. II A. Based on the thermodynamics of an ensemble of particles described in Sec. II B, we formulate the theory of population dynamics based on the generalized Fokker-Planck equation and the Langevin equation in Sec. II C. In Sec. II E we compute numerically and approximate analytically the condition for mosaic instability and observe its strong dependence on the reaction kinetics. Section III applies the theory to Li-ion batteries and a model system at the critical point.

II. THEORY

A. From single-particle dynamics to population dynamics

We begin by considering a particle that undergoes reactions when it is out of chemical equilibrium with its surroundings,

$$M_{\text{res}} \rightarrow M, \tag{1}$$

where the single component of interest M reacts with a reservoir with species M_{res}. The dynamics is described by the change in the concentration of M in the particle,

$$\frac{dc}{dt} = R(c, \mu, \mu_{\text{res}}), \tag{2}$$

where R is the reaction rate as a function of concentration c and the chemical potential of M in the particle μ and of M_{res} in the reservoir μ_{res}. The reaction rate is zero at chemical equilibrium $\mu = \mu_{\text{res}}$.

Following Bazant [13], we define the total autocatalytic rate of the reaction to be

$$s = \frac{\partial R}{\partial c} = \left(\frac{\partial R}{\partial c}\right)_{\mu} + \left(\frac{\partial R}{\partial \mu}\right)_{c} \frac{d\mu}{dc}, \tag{3}$$

which determines whether the concentration profile is linearly stable ($s < 0$) or unstable ($s > 0$) to infinitesimal perturbations. (See Ref. [13] for a general stability theorem for multicomponent driven reactive mixtures in terms of the chemical diffusivity and autocatalytic rate tensors.) In most classical theories, the reaction rate is linear in the thermodynamic driving force or affinity of the reaction [40]. More generally, if the reaction rate is linearized near equilibrium $R = R_0 \Delta\mu$, for small thermodynamic driving force $\Delta\mu = \mu_{\text{res}} - \mu$ with constant prefactor R_0, the autocatalytic rate is given by $s = -R_0\, d\mu/dc$. In this case of near-equilibrium reactions, we arrive at the Duhem-Jougeut theorem [40], which states that kinetic stability ($s < 0$) is equivalent to thermodynamic stability ($d\mu/dc > 0$).

Far from equilibrium, the situation is very different, and kinetic stability is altered by the explicit dependence of the reaction rate on concentration or chemical potential [13]. The concentration profile tends to be destabilized by a positive solo autocatalytic rate $(\partial R/\partial c)_{\mu} > 0$ or, in the case of a thermodynamically stable system $d\mu/dc > 0$, by a negative differential reaction resistance $(\partial R/\partial \mu)_{c} < 0$ (as in the case of Marcus kinetics for electron transfer reactions [14]).

The analysis of kinetic stability described here is applicable to lithium intercalation reaction in LFP, a phase-separating

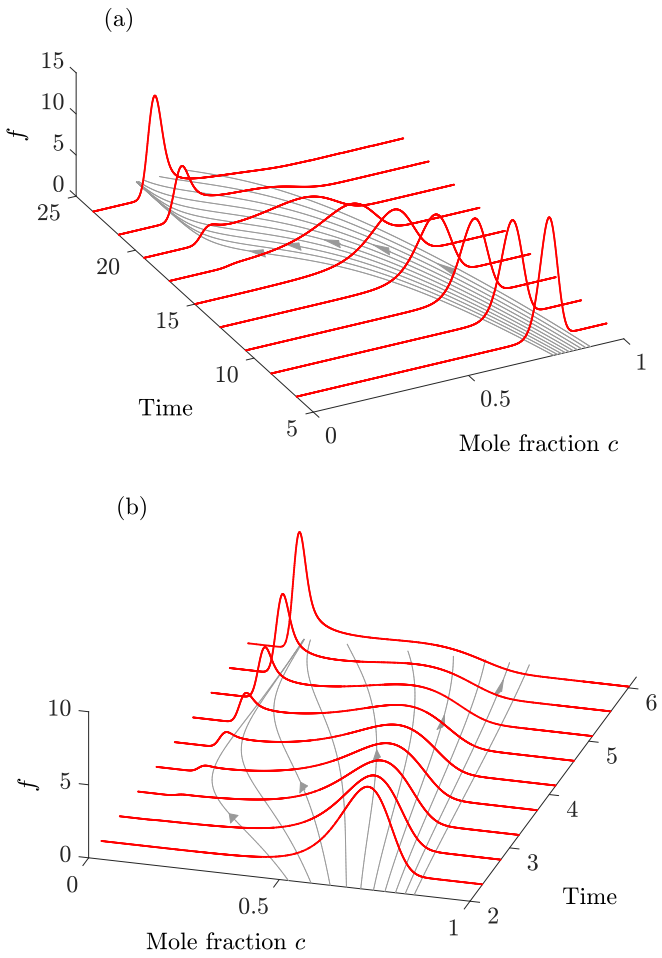

FIG. 1. Evolution of the probability distribution $f(c, t)$ in time ($D_0 = 10^{-3}$), shown by the red curves. The system undergoes a reaction at (a) constant external reservoir chemical potential and (b) constant total reaction rate with time-dependent reservoir chemical potential. The gray curves on the horizontal plane are characteristics of, or solutions to, the deterministic reaction rate equation $dc/dt = R$ starting from different initial conditions. The distribution widens where characteristics diverge due to autocatalysis and it sharpens where characteristics converge due to autoinhibition.

electrode material. Bazant and co-workers [14,41,42] showed a linearly stable regime in the spinodal region at large enough reaction rate, leading to the suppression of phase separation. The reaction kinetics has been coupled with phase field and mechanical models to predict the spatial pattern of lithium concentration within nanoparticles [35,41–44].

In the limit of vanishing spatial gradient within particles, the models above for lithium intercalation reduce to Eq. (2). In the limit of an infinite number of reaction-controlled particles that are small enough to assume intraparticle homogeneity, we switch from a Lagrangian description of the discrete particle dynamics to an Eulerian description in terms of a probability distribution

$$\frac{\partial f}{\partial t} + \frac{\partial (fR)}{\partial c} = 0, \tag{4}$$

where $f(t, c)$ is the probability distribution function (PDF).

The characteristics of the linear advection equation in the c-t space is given by the reaction kinetics in Eq. (2) [1]. When the reaction is autocatalytic $\partial R/\partial c > 0$, characteristics diverge and the distribution expands, whereas when $\partial R/\partial c < 0$, characteristics converge and the distribution forms a shock. Figure 1 illustrates the effect of autocatalysis on the evolution of $f(t, c)$ for two cases where a unimodal distribution evolves into a bimodal distribution over time. The evolution of $f(t, c)$ follows the characteristics, or the gray curves, which are solutions to Eq. (2). Due to autocatalysis, particles ahead of others in the reaction direction accelerate and form another peak in the PDF around a concentration removed from the original peak.

B. Thermodynamics of a particle ensemble

The model above assumes a deterministic reaction rate. Now we seek a statistical mechanical description for an ensemble of particles, where thermodynamic fluctuations are important. For simplicity, we consider single-component systems. In the canonical ensemble, the number of M in the system is fixed to be N. In the grand canonical ensemble, the system is in a chemical reservoir of $M_{\rm res}$ with chemical potential $\mu_{\rm res}$. In Table I we define thermodynamic quantities in canonical and grand canonical ensembles as a function of the probability distribution [45]: p_ν is the probability of a particular microstate ν, $p_{\nu_N} = p(\nu|N)$ is the conditional probability of a microstate given N molecules, and p_N is the marginal probability of having N molecules. The probability distribution can be generally in or out of equilibrium. For the canonical ensemble, the subscripts N in the free energy A_N, average energy $\langle E\rangle_N$, and entropy S_N denote the number of molecules specified for the ensemble. We are particularly interested in how the thermodynamic quantities in the grand canonical ensemble are associated with those in the canonical ensemble. For example, using the property of conditional probability $p_\nu = p_{\nu_N} p_N$, the grand canonical entropy S, the canonical entropy S_N, and the entropy due to chemical fluctuations S' are related by

$$S = S' + \langle S_N\rangle, \tag{5}$$

where $\langle S_N\rangle = \sum_N p_N S_N = -k_{\rm B}\sum_\nu p_\nu \ln p_{\nu_N}$ is the canonical entropy averaged over N and is also known as conditional entropy in information theory.

The free energies of the two ensembles are also related as shown in Table I. In particular, if all degrees of freedom except for N are at equilibrium, the grand canonical ensemble free energy is

$$\Psi = \sum_N p_N\left(A_N^{\rm eq} - \mu_{\rm res}N + k_{\rm B}T\ln p_N\right). \tag{6}$$

This may describe the free energy of an ensemble of particles that have reached equilibrium within themselves but not necessarily with the reservoir.

For convenience, we use $A = A_N^{\rm eq}$ to denote the canonical ensemble free energy at equilibrium. From thermodynamics, the system is stable when $\partial^2 A/\partial N^2 > 0$, if N is treated as a continuous variable. An example of instability, which leads to phase separation, can arise in the lattice model discussed in Sec. II E. Since the chemical potential of M within the particle is defined as $\mu = \partial A/\partial N$, the stability criterion can also be written as $\partial\mu/\partial N > 0$. This is not to be confused with the fact that, at equilibrium, $\partial^2\Psi^{\rm eq}/\partial\mu_{\rm res}^2 = -\partial\langle N\rangle^{\rm eq}/\partial\mu_{\rm res} = -k_{\rm B}T\sigma_N^2 < 0$, where σ_N^2 is the variance of N. Therefore, at equilibrium, the average number of M in a grand canonical ensemble always increases with reservoir chemical potential regardless of A. Note that σ_N^2 at equilibrium is constructed naturally as a result of the entropy S' associated with chemical fluctuations.

TABLE I. Definitions of thermodynamic quantities. Angular brackets denote averaging over states in the summation that comes immediately before its appearance. Here $\beta = 1/k_{\rm B}T$.

Ensemble type	Free energy	Entropy
canonical	$A_N = \sum_{\nu_N} p_{\nu_N}(E_{\nu_N} + k_{\rm B}T\ln p_{\nu_N})$ $= \langle E\rangle_N - TS_N$	$S_N = -k_{\rm B}\sum_{\nu_N} p_{\nu_N}\ln p_{\nu_N}$
grand canonical	$\Psi = \sum_\nu p_\nu(E_\nu - \mu_{\rm res}N_\nu + k_{\rm B}T\ln p_\nu)$ $= \langle E\rangle - \mu_{\rm res}\langle N\rangle - TS$ $= \sum_N p_N(A_N - \mu_{\rm res}N + k_{\rm B}T\ln p_N)$ $= \langle A_N\rangle - \mu_{\rm res}\langle N\rangle - TS'$	$S = -k_{\rm B}\sum_\nu p_\nu\ln p_\nu$ $S' = -k_{\rm B}\sum_N p_N\ln p_N$
Ensemble type	**Equilibrium distribution**	
canonical	$p_{\nu_N}^{\rm eq} = \exp\left[-\beta(E_{\nu_N} + A_N^{\rm eq})\right]$	
grand canonical	$p_\nu^{\rm eq} = \exp[-\beta(E_\nu + \mu_{\rm res}N_\nu + \Psi^{\rm eq})]$, $p_N^{\rm eq} = \exp\left[-\beta(A_N^{\rm eq} + \mu_{\rm res}N + \Psi^{\rm eq})\right]$	

At equilibrium, the probability distribution satisfies the Boltzmann distribution and minimizes the free energy. Therefore, we define a Lyapunov function below in Eq. (7). It is always greater than or equal to zero and, as will be shown later, monotonically decreases for systems with a constant $\mu_{\rm res}$. The Lyapunov function is called relative entropy, or Kullback-Leibler divergence, which originates in information theory to measure the difference between two probability distributions

$$\mathcal{L} = \Psi - \Psi^{\rm eq} = k_{\rm B}T \sum_{\nu} p_\nu \ln \frac{p_\nu}{p_\nu^{\rm eq}} > 0. \tag{7}$$

C. Dynamics

In the classical limit, we use a general continuous variable $\mathbf{x}$ that maps the microstate of the system ν to $\mathbb{R}^n$ and use p to denote the probability density function. In the grand canonical ensemble, equilibrium corresponds to $\delta\Psi/\delta p = E - \mu_{\rm res}N + k_{\rm B}T \ln p$ being a constant subject to the normalization condition for p. Based on Wasserstein gradient flow [28,46,47] that drives the probability distribution toward minimum energy, we obtain the Fokker-Planck equation

$$\frac{\partial p}{\partial t} + \nabla \cdot \mathbf{J} = 0, \tag{8}$$

where

$$\mathbf{J} = -\mathbf{K}p\nabla\frac{\delta\Psi}{\delta p} = -\mathbf{K}k_{\rm B}T\, p\nabla \ln \frac{p}{p^{\rm eq}}, \tag{9}$$

with $\mathbf{K}$ the mobility tensor.

The following second law of thermodynamics is well known in stochastic thermodynamics [30,48–53],

$$\frac{d\Psi}{dt} = -\int_{\mathbb{R}^n} \frac{\mathbf{J}^\dagger \mathbf{K}^{-1}\mathbf{J}}{p} d\mathbf{x} + \int_\Omega p\frac{d}{dt}(E - \mu_{\rm res}N) d\mathbf{x}, \tag{10}$$

where the first term is the entropy production rate $-T\dot{S}_i$ and the second term is the work of external driving force $\dot{W}_d$. When the system is driven chemically,

$$\dot{W}_d = -\dot{\mu}_{\rm res}\langle N\rangle. \tag{11}$$

The second law of thermodynamics requires that $\dot{S}_i > 0$, or equivalently that $\mathbf{K}$ be positive definite. When the system is nondriven, $\Psi - \Psi^{\rm eq}$ decreases monotonically, hence it is a Lyapunov function.

If the relaxation of its internal degrees of freedom ν_N to equilibrium is much faster than the exchange of matter with the reservoir, we assume all internal degrees of freedom are at equilibrium, that is, $p_\nu = p^{\rm eq}_{\nu_N} p_N$. In this case, the marginal probability p_N follows

$$\frac{\partial p_N}{\partial t} + \frac{\partial J_N}{\partial N} = 0, \tag{12}$$

where

$$J_N = -(\mathbf{K})_{N,N} p_N \frac{\partial}{\partial N}\left(\frac{\delta\Psi}{\delta p_N}\right), \tag{13}$$

$$\frac{\delta\Psi}{\delta p_N} = A_N^{\rm eq} - \mu_{\rm res}N + k_{\rm B}T \ln p_N. \tag{14}$$

As discussed in Refs. [54–56], the chemical Langevin equation and the corresponding Fokker-Planck equation can be derived from the chemical master equation in the length scale and timescale we are interested in for an ensemble of mesoscopic particles. This justifies the switching from discrete to continuous N. We show below that the chemical Fokker-Planck equation derived here satisfies detailed balance.

For concentrated solutions, it is convenient to nondimensionalize the number of molecules N in the system by the its maximum N_t. Assuming that N_t is fixed, the equation can be nondimensionalized via the mole fraction $c = N/N_t$, the PDF in terms of c, $f = P_N N_t$, and the prefactor $k = (\mathbf{K})_{N,N}/N_t$. In contrast to linear kinetics, k can be a function of c, μ, and $\mu_{\rm res}$ and we do not make any assumption about the functional form other than $k > 0$,

$$\frac{\partial f}{\partial t} + \frac{\partial[(\mu_{\rm res} - \mu)kf]}{\partial c} = \frac{k_{\rm B}T}{N_t}\frac{\partial}{\partial c}\left(k\frac{\partial f}{\partial c}\right), \tag{15}$$

where $\mu = \partial A_N^{\rm eq}/\partial N$. Alternatively,

$$\frac{\partial f}{\partial t} + \frac{\partial j}{\partial c} = 0, \tag{16}$$

where the flux j is

$$j = \left((\mu_{\rm res} - \mu)k - k\frac{k_{\rm B}T}{N_t}\frac{\partial}{\partial c}\right)f = kk_{\rm B}T f^{\rm eq}\frac{\partial}{\partial c}\left(\frac{f}{f^{\rm eq}}\right), \tag{17}$$

where $f^{\rm eq}$ is the equilibrium distribution, given by Eq. (19). Defining the maximum number of molecules N_t restricts the fraction $c \in [0, 1]$. Therefore, we impose the no-flux boundary condition $j = 0$ at $c = 0$ and 1. To be compatible, we require the chemical potential $\mu \to \infty$ as $c \to 1$ and $\mu \to -\infty$ as $c \to 0$ and it is undefined outside (0,1).

Following the nondimensionalization, we define the free energy

$$\Psi_m = \int_0^1 \left(a - \mu_{\rm res}c + \frac{k_{\rm B}T}{N_t}\ln f\right) f\, dc, \tag{18}$$

where $a = A/N_t$. Following the analysis of the general case (8), Ψ_m is the Lyapunov function for Eq. (15). Therefore, if not chemically driven, or at constant $\mu_{\rm res}$, the system is Lyapunov stable. In fact, it can also be shown that the eigenvalues of the operator $(\mu_{\rm res} - \mu)k - kk_{\rm B}TN_t^{-1}\partial/\partial c$ are non-negative, and $f^{\rm eq}$ corresponds to the zero eigenvalue [46]. In other words, the equilibrium distribution corresponds to $\partial j/\partial c = 0$, or $j = 0$, based on the boundary condition

$$f^{\rm eq}(c) = e^{-\beta N_t(a - \mu_{\rm res}c - \Psi_m^{\rm eq})}, \tag{19}$$

where $\Psi_m^{\rm eq}$ is the potential defined in Eq. (18) when at equilibrium and is the constant that satisfies the normalization condition for f.

By comparing Eqs. (4) and (15), we find that the reaction rate is $R = (\mu_{\rm res} - \mu)k$. In the limit of large systems $N_t \to \infty$, Fokker-Planck equation (15) reduces to Eq. (4). The reaction rate defined here naturally follows detailed balance. Now we are able to correlate chemical fluctuations with the diffusive term in the Fokker-Planck equation and extend the deterministic reaction rate, or Eq. (2), to the equivalent Langevin

equation

$$\frac{dc}{dt} = R + \sqrt{2\frac{k_B T k}{N_t}}\xi(t), \tag{20}$$

where the Langevin noise $\xi(t)$ has zero average $\langle\xi(t)\rangle = 0$ and is uncorrelated in time $\langle\xi(t)\xi(t')\rangle = \delta(t-t')$. Equation (15) can also be written as

$$\frac{\partial f}{\partial t} + \frac{\partial (fR)}{\partial c} = \frac{\partial}{\partial c}\left(D\frac{\partial f}{\partial c}\right), \tag{21}$$

where $D = k_B T k/N_t$ is an expression of the Einstein relation or fluctuation-dissipation theorem for concentration fluctuations across the particle ensemble. The noise intensity decreases as the size of the particle increases.

D. Evolution of the concentration variance

In Sec. II A we mentioned that when $\partial R/\partial c > 0$, characteristics diverge and the probability distribution spreads. This statement can be made more quantitative in the case of non-negligible fluctuations by considering the evolution of the concentration variance. Herrmann *et al.* [28] analyzed the spreading in the unstable region where $\partial\mu/\partial c < 0$ by linearizing the reaction R with respect to c, which specifically entails linearizing the chemical potential μ since the prefactor k is assumed to be constant. Therefore, in this case, the widening of the distribution is determined by $\partial\mu/\partial c$. The analysis requires that the distribution be sharply peaked. With the same assumption, we extend the analysis to a general reaction rate expression and approximate the evolution of the concentration variance $\sigma_c^2 = \int_0^1 (c-c_0)^2 f(c)dc$. The distribution $f(t,c)$ satisfies Eq. (16) with $j = fR - k_B T N_t^{-1} k\partial f/\partial c$. We define the mean $c_0 = \langle c\rangle$, and the evolution of the concentration variance is

$$\begin{aligned}\frac{d\sigma_c^2}{dt} &= \frac{d}{dt}\left(\int_0^1 (c-c_0)^2 f\, dc\right)\\ &= \int_0^1 (c-c_0)^2\frac{\partial f}{\partial t}dc = 2\int_0^1 j(c-c_0)dc.\end{aligned} \tag{22}$$

We expand the current j about c_0 and use the superscript (m) to define the mth derivative with respect to c,

$$\begin{aligned}j = f&\left(\sum_{m=0}^{\infty} R^{(m)}(c_0)\frac{(c-c_0)^m}{m!}\right)\\ &- \frac{k_B T}{N_t}\left(\sum_{m=0}^{\infty} k^{(m)}(c_0)\frac{(c-c_0)^m}{m!}\right)\frac{\partial f}{\partial c},\end{aligned} \tag{23}$$

therefore,

$$\begin{aligned}\frac{d\sigma_c^2}{dt} &= 2\sum_{m=0}^{\infty} R^{(m)}(c_0)\frac{\langle(c-c_0)^{m+1}\rangle}{m!}\\ &\quad + 2\frac{k_B T}{N_t}\sum_{m=0}^{\infty} k_0^{(m)}\frac{m+1}{m!}\langle(c-c_0)^m\rangle.\end{aligned} \tag{24}$$

If f is concentrated around c_0, higher-order moments in the expression (24) decay very quickly and are negligible. Therefore, we retain only moments up to $\langle(c-c_0)^2\rangle = \sigma_c^2$. In the limit of the sharply peaked distribution, $k_B T/N_t$ and σ_c^2 are both small and we arrive at the key result

$$\frac{d\sigma_c^2}{dt} = 2\left(\left.\frac{\partial R}{\partial c}\right|_{c_0}\sigma_c^2 + \frac{k_B T}{N_t}k_0\right), \tag{25}$$

where $k_0 = k(c_0)$ and $c_0 = \langle c\rangle$ is the average mole fraction. Autoinhibitory reactions ($\partial R/\partial c < 0$) decrease the spread in particle concentration. Autocatalytic reactions lead to greater heterogeneity.

If the equilibrium distribution is unimodal with a sharp peak, it can be approximated by a normal distribution by expanding the free energy a in terms of c to second order,

$$f^{\mathrm{eq}}(c) \approx e^{-\beta N_t \mu'(c_0)(c-c_0)^2/2} e^{-\beta N_t\left[a(c_0)-\mu(c_0)c_0-\Psi_m^{\mathrm{eq}}\right]}, \tag{26}$$

where $\mu_{\mathrm{res}} = \mu(c_0)$ and $\sigma_c^2 = k_B T/N_t\mu'(c_0)$. The same conclusion is obtained by setting Eq. (25) to zero, since $\partial R/\partial c = -k_0\partial\mu/\partial c + (\mu_{\mathrm{res}} - \mu)\partial k/\partial c$. When the system is thermodynamically stable ($\partial\mu/\partial c > 0$), the variance can become greater or smaller than the equilibrium variance when there is a net reaction, depending on the sign of $\partial k/\partial c$ and the direction of the net reaction. The next section describes how different $k(c)$ models result in different population dynamics behavior.

In the limit of negligible fluctuations $N_t \to \infty$, Eq. (25) gives the evolution of variance over time,

$$\sigma_c^2(t) = \sigma_c^2(t=0)\exp\left(2\int_0^t \frac{\partial R}{\partial c}dt\right). \tag{27}$$

In the same limit, with the initial condition $f(c_0, t=0) = f_0(c_0)$, using the method of characteristics, the solution to the Fokker-Planck equation without the diffusive term (4) is [1]

$$f(c(t,c_0),t) = f_0(c_0)\exp\left(\int_0^t -\frac{\partial R}{\partial c}(c(t,c_0),t)dt\right), \tag{28}$$

where $c(t,c_0)$ follows the characteristics and is the solution to Eq. (2) with the initial condition $c(t) = c_0$. We see that, in the limit of a sharply peaked distribution, by taking the variance on both sides of Eq. (28), Eq. (27) is recovered. If the reaction rate does not explicitly depend on t, then

$$f(c(t,c_0),t) = f_0(c_0)\frac{R(c_0)}{R(c(t,c_0),t)}. \tag{29}$$

E. Electrochemical reactions

As a benchmark for the population dynamics model, in this section we focus on the effect of reaction kinetics in the context of electrochemical reactions. We impose a constant total reaction rate, or constant current,

$$R_{\mathrm{total}} = \frac{d\langle c\rangle}{dt} = \int_0^1 c\frac{\partial f}{\partial t}dc = \int_0^1 j\, dc. \tag{30}$$

In the limit of a sharply peaked distribution, the center of the peak c_0 is equal to the average concentration $\langle c\rangle$ and shifts linearly in time. The total reaction rate is equal to the reaction rate at c_0, that is, $dc_0/dt = R(c_0)$. Therefore, the evolution of

variance in Eq. (25) can also be written as

$$\frac{d\sigma_c^2}{dc_0} = 2\left(\frac{s}{R}\Big|_{c_0}\sigma_c^2 + \frac{k_BT}{N_t}\frac{1}{\mu_{res}-\mu}\right). \tag{31}$$

In the limit of negligible fluctuation or infinitely large reaction rate, when the thermodynamic driving force $|\mu_{res}-\mu|$ is large, the growth of the standard deviation of the distribution is given by

$$K = \ln\left(\frac{\sigma_c}{\sigma_{c_0}}\right) = \int_{c_0}^{c}\frac{s}{R}dc. \tag{32}$$

In this section, we consider the simple reaction kinetics

$$R = R_0(c)g(\mu_{res}-\mu), \tag{33}$$

where $g(0) = 0$, which includes important cases of electrochemical reactions [13,14]. The corresponding autocatalytic rate is

$$s = \frac{\partial R}{\partial c} = R_0'g - R_0g'\mu' = R\left(\frac{R_0'}{R_0} - \frac{g'}{g}\mu'\right). \tag{34}$$

With this particular form of reaction kinetics, we have

$$K = \ln R_0|_{c_0}^{c} - \int_{c_0}^{c}\frac{g'}{g}\mu' dc. \tag{35}$$

Here we focus on the explicit dependence of the reaction rate on concentration, in particular how the exchange current $R_0(c)$ affects the stability of the particle ensemble by autocatalysis [13]. Hence we discuss the case of positive differential resistance $g' > 0$, that is, the reaction rate increases with the driving force, which preserves the contribution of the thermodynamic stability to the overall stability. Although not the focus of the paper, the Marcus theory for outer-sphere electron transfer, for example, exhibits an inverted region, or negative differential resistance [13,14], which can destabilize a thermodynamically stable system and make the reaction autocatalytic. Reaction kinetics of this form can be derived from transition state theory. For example, the famous Butler-Volmer equation has the form above [14,57], where R_0 is called the exchange current and

$$g(x) = e^{\alpha x} - e^{-(1-\alpha)x}, \tag{36}$$

where α is the charge transfer coefficient. In the case of symmetric Butler-Volmer kinetics, $\alpha = 0.5$ and $g' = \sqrt{(g/2)^2+1}$. The standard deviation grows in regions where $s > 0$, or $(\ln R_0)' > \sqrt{1/4 + (R_0/R)^2}\mu'\mathrm{sgn}(R)$, as shown by Bazant in Ref. [13]. With Butler-Volmer kinetics, when the driving force $|\mu_{res}-\mu|$ is small, $g(x) \to x$ and the reaction rate is slow. Therefore, the second term in Eq. (32) dominates and whether the standard deviation increases or decreases is mainly determined by the thermodynamic stability

$$K \approx -\frac{1}{R}\int_{c_0}^{c} R_0\mu' dc. \tag{37}$$

At high total reaction rate, both the exchange current and thermodynamics determine the evolution of standard deviation.

$$K \approx \ln R_0|_{c_0}^{c} - \begin{cases}\alpha\mu|_{c_0}^{c} & \text{if } R > 0\\ -(1-\alpha)\mu|_{c_0}^{c} & \text{if } R < 0.\end{cases} \tag{38}$$

The exchange current of the reaction kinetics is crucial in determining the stability of the system [13,19]. The asymmetry in exchange current leads to asymmetric behavior between forward and backward reactions. In the case of LFP, a skewed exchange current results in more uniform concentration profiles during intercalation and greater inhomogeneity during deintercalation. To illustrate how the exchange current affects the stability, we choose the regular solution as the thermodynamic model

$$\frac{\mu}{k_BT} = \ln\frac{c}{1-c} + \Omega(1-2c), \tag{39}$$

where the first term arises from the entropy of mixing and the second term comes from the enthalpic interaction. When $\Omega > 2$, the system phase separates into two phases with low and high concentrations.

Table II lists, in the case of symmetric Butler-Volmer kinetics ($\alpha = 0.5$), the maximum standard deviation ratio at an infinitely fast reaction rate for three types of exchange current, which is attained in the interval $[c_1, c_2]$ in which $\partial R/\partial c \geqslant 0$. The starting and ending concentrations c_1 and c_2 are also listed in the table. See Sec. III A below for a plot and discussion of the region of instability $\partial R/\partial c \geqslant 0$ at arbitrary reaction rates. The first two exchange currents are symmetric and thus exhibit symmetric behavior for forward and backward reactions. A constant exchange current does not alter the stability: The unstable region ($s > 0$) is exactly the spinodal region ($\partial\mu/\partial c > 0$), which exists when $\Omega > 2$. Figure 2 shows the evolution of the standard deviation at an infinitely large reaction rate. The third row of the figure shows that the evolution for the constant exchange current follows the trend of the chemical potential. For the second exchange current $\sqrt{c(1-c)}$, which is frequently used in electrochemistry, the standard deviation grows within $[0, 1-1/\Omega]$ for the forward reaction and $[1/\Omega, 1]$ for the backward reaction. The unstable region exists when $\Omega > 1$. Since at low enough reaction rate the system always follows thermodynamic stability, when $1 < \Omega < 2$ it only becomes linearly unstable at a high reaction rate. As shown in the second row of Fig. 2, the second exchange current results in a larger maximum standard

TABLE II. Maximum standard deviation ratio with the starting and ending average fractions for three different exchange currents.

Exchange current	1 ($\Omega > 2$)	$\sqrt{c(1-c)}$ ($\Omega > 1$)	$(1-c)e^{\mu/2}$ ($\Omega > \frac{1}{2}$)
$\max_{c_1,c_2}\frac{\sigma_{c_1}}{\sigma_{c_2}}$	$\frac{1-\sqrt{1-2/\Omega}}{1+\sqrt{1-2/\Omega}}\exp(\Omega\sqrt{1-2/\Omega})$	$\frac{1}{\Omega}e^{\Omega-1}$	$\frac{1}{2\Omega}e^{2\Omega-1}$
c_1	$\frac{1\mp\sqrt{1-2/\Omega}}{2}$	0 or 1	1
c_2	$\frac{1\pm\sqrt{1-2/\Omega}}{2}$	$1-\frac{1}{\Omega}$ or $\frac{1}{\Omega}$	$\frac{1}{2\Omega}$

deviation ratio as well as region of instability than the constant exchange current.

As Bazant has shown [13], the third exchange current is predominantly autocatalytic in the backward direction due to the asymmetrically increasing exchange current in that direction. When the direction is reversed, the autoinhibition results in greater homogeneity for the forward reaction. In particular, at an infinitely large backward reaction rate, the system is kinetically unstable within the concentration range

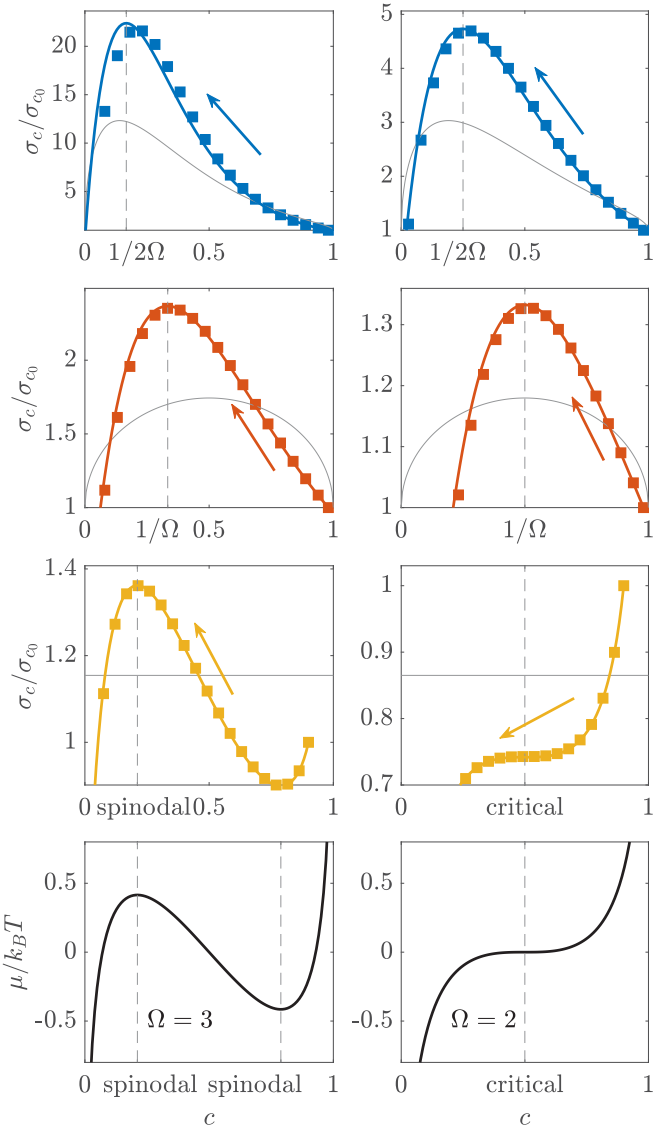

FIG. 2. Evolution of the standard deviation of the distribution at infinitely large negative reaction rate and zero fluctuation. The colored solid curves plot the analytical expression (38). Squares represent simulations at sufficiently large negative currents. The location of maximum standard deviation is marked by dashed lines and is predicted in Table II. Each row corresponds to a different exchange current shown in gray solid curves. The regular solution is used as the thermodynamic model. The left column corresponds to $\Omega = 3$, a phase-separating system. The right column corresponds to $\Omega = 2$, which is at the critical point. The arrows indicate the direction of reaction as well as the autocatalytic effect in the case of increasing standard deviation.

$[1/2\Omega, 1]$, which exists when $\Omega > 1/2$. At an infinitely large forward reaction rate, the system remains stable regardless of the value of Ω, behaving entirely differently from the symmetric exchange currents. Figure 2 shows that, in the backward direction, the amplification of standard deviation and the width of the instability interval increases in the order of constant, symmetric $\sqrt{c(1-c)}$, and asymmetric $(1-c)e^{\mu/2}$ exchange current, the reason for the latter being $1/2\Omega < (1-\sqrt{1-2/\Omega})/2 < 1/\Omega$. Figure 2 also shows the agreement between the analytical expression for the evolution of standard deviation from Eq. (38) and numerical simulation for the same exchange currents. The approximation captures the magnitude of maximum standard deviation and where maximum standard deviation is attained.

When the variance σ_c^2 is large, the assumption of a sharply peaked distribution no longer holds. For example, when the system is driven toward a high concentration, an autocatalytic effect may cause some particles to accelerate to much higher concentration than average. However, the highest concentration a particle can reach is the equilibrium concentration corresponding to μ_{res}. The stabilizing effect of thermodynamics when the concentration is near equilibrium ($\partial R/\partial c > 0$) causes those particles to form another peak in the distribution. We define the resulting bimodal distribution to be mosaic instability.

The key result of this work is to show that mosaic instability can arise as a result of both kinetic and thermodynamic effects, and mathematically it is a result of diverging and converging characteristics. Based on the analysis, we may approximate the initiation of mosaic instability as when the estimated variance $\sigma_c = \sigma_{c_0}e^K$ exceeds a certain threshold, where σ_{c_0} can be taken at the inception of linear instability or the initial condition, when, as explained previously, the magnitude of standard deviation is proportional to the strength of the random fluctuation, that is, $\sigma_{c_0} \propto \sqrt{D}$. In the case of linear kinetics with constant exchange current, that is, $R = R_0(\mu_{\text{res}} - \mu)$, where R_0 is a constant, we have $K = [\mu(c) - \mu(c_0)]R_0/R$. Thus, we obtain the following critical current R_c above which a thermodynamically phase-separating system is kinetically stabilized, consistent with the conclusion of Herrmann *et al.* [28]:

$$\frac{R_c}{R_0} \propto \frac{1}{\ln 1/\sqrt{D}}. \tag{40}$$

III. APPLICATIONS

A. Li-ion battery porous electrodes

We first look at the example of lithium iron phosphate, one of the most well-studied phase-separating solid-state lithium intercalation materials. The lithiation reaction is $Li^+ + e^- + FePO_4 \rightarrow LiFePO_4$ and the reverse reaction is called delithiation. The chemical potential of lithium in the solid can be modeled by the regular solution model given by Eq. (39) as a function of the lithium fraction in the solid, with $c = 0$ being $FePO_4$ and $c = 1$ being $LiFePO_4$. We model the population dynamics using (a) a classical exchange current $\sqrt{c(1-c)}$, (b) exchange current derived from transition state theory $(1-c)e^{\mu/2}$, and (c) an experimentally measured exchange current [19], all with Butler-Volmer kinetics.

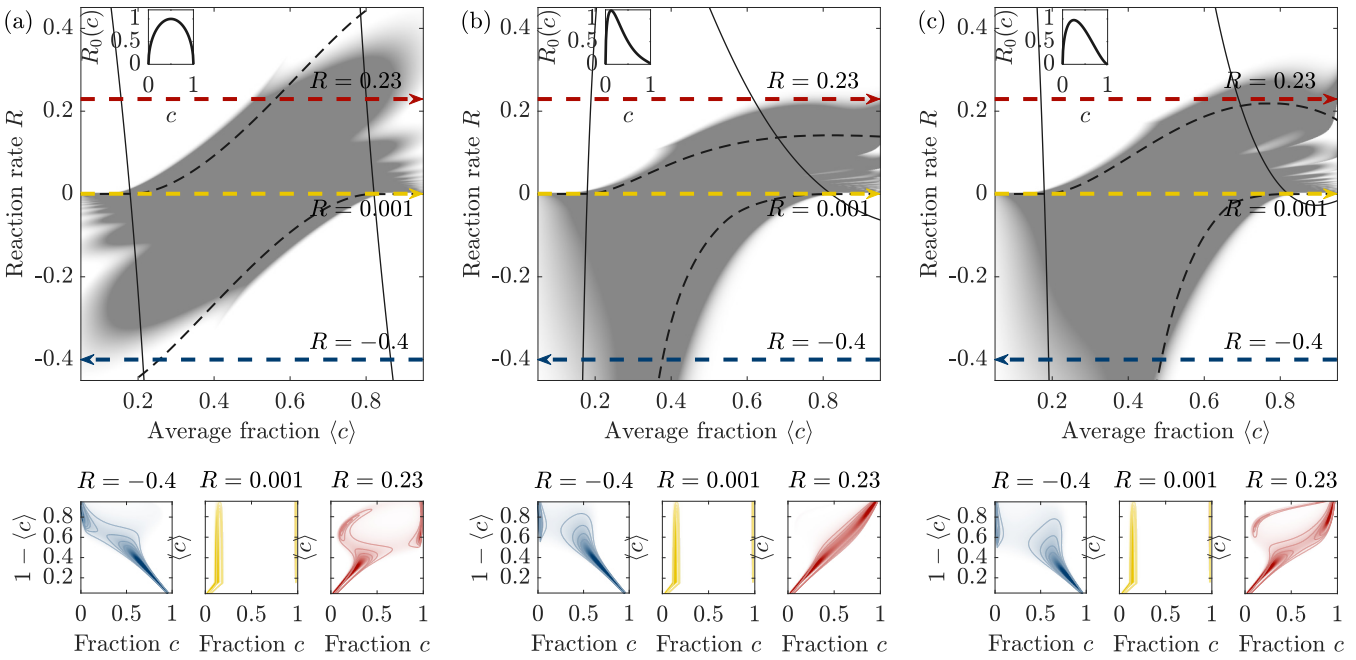

FIG. 3. Population dynamics applied to a lithium iron phosphate electrode. The main plots show the degree of mosaic instability as a function of the current applied and average fraction. The prominence of the second peak in $f(t, c)$ is equal to or greater than 1 for the most intense gray color and 0 for white. The plots below show the evolution of the probability distribution in time at a certain constant current whose trajectory is denoted by the same color in the main plot. The value $f(t, c)$ is equal to or greater than 10 at the greatest intensity and 0 for white. The thermodynamics is modeled by the regular solution model ($\Omega = 3.4$ and $D_0 = 2 \times 10^{-4}$). Insets show the exchange current $R_0(c)$. Within the solid black curves, the system is linearly unstable $\partial R/\partial c > 0$. Dashed lines encircle the predicted region of mosaic instability using Eq. (41).

In this section we focus on the population dynamics of an ensemble of LFP particles under constant current. Figure 3 shows the dynamic phase diagram of the LFP model as a function of current and average Li fraction and the evolution of the probability distribution function in time at select currents. With a positive current (reaction rate), the average Li fraction increases, which corresponds to going horizontally from left to right in the main figure and vice versa for a negative current. In the preceding section we defined mosaic instability to be when the PDF is bimodal. This is shown by the gray area in the main plot. The color indicates the prominence of the second largest peak, which qualitatively measures the degree of mosaic instability. To clearly mark the mosaic instability region, the color is saturated when the value is greater than 1. The point of exit from mosaic instability is oscillatory with respect to the total reaction rate. This is due to the varying frequency observed in the regime of oscillatory phase transition, which was previously addressed extensively and is beyond the scope of this work [15,28,29].

At low currents, regardless of the exchange current, thermodynamics drives the particle ensemble to separate into Li-poor and Li-rich populations, which correspond to growing and shrinking peaks seen at $i/i_0 = 10^{-3}$. As shown in the dynamic phase diagram, at low currents (but not $R \to 0$, as explained below), the mosaic instability initiates at around the nearest spinodal point.

As mentioned above, Herrmann and co-workers [15,28,29] performed extensive analysis on the various regimes of the population dynamics at different currents for the simple kinetics $R = R_0 \Delta\mu$. Our more general model approaches it asymptotically as $R \to 0$. In Kramer's regime, the reaction rate is proportional to $\exp(-b/D)$, where b is the free-energy barrier, or the difference between the local maximum and minimum of $a - \mu_{\text{res}} c$. Since the reaction rate is equal to the rate of phase transformation in this regime, as b/D increases, the rate of nucleation decreases exponentially. To reach the quasistationary limit, that is, for the phase-separating region to span between the two thermodynamic phases (binodal points), the rate must be smaller than Kramer's rate at the largest possible free-energy barrier ($\mu_{\text{res}} = 0$), which is around 10^{-422} for the particular set of parameters chosen ($\Omega = 3.4$ and $D_0 = 2 \times 10^{-4}$); therefore, the dynamic phase diagram shown is effectively only for current at or above Kramer's regime and the system must at least reach the spinodal point for the nucleation to occur.

The solid curves denote the boundary of linear instability, $s = 0$. In between the two curves, $s > 0$. At zero current, the region of linear instability is also the spinodal region. The region of mosaic instability does not follow the shape of the region of linear instability. In fact, nucleation is delayed with increasing current. We seek an approximation for the region of mosaic instability. When mosaic instability occurs, the newly formed phase is close to $c = 1$ for $R > 0$ and close to $c = 0$ for $R < 0$. Therefore, we approximate the single-phase behavior to be when the spread of the distribution (which is approximately one standard deviation $\sigma_c = \sigma_{c_0} e^K$) is within [0,1],

$$0 < c \pm \sigma_c < 1. \tag{41}$$

For a qualitative understanding, we choose an order-of-magnitude estimate for the initial variance $\sigma_{c_0} = \sqrt{D}$. Here c_0 is the first point where $s = 0$ or the initial average concentration used in the simulation (0.05 or 0.95), whichever comes later in the direction of the reaction. The predicted region of mosaic instability is bounded by the dashed lines. This simple approximation captures the general feature of the boundary of mosaic instability. The form of reaction kinetics, in particular the autocatalytic rate $\partial R/\partial c$, is the dominant factor in determining the mosaic instability region. It also indicates that the delayed nucleation is mainly due to decreasing s/R with increasing reaction rate.

The regimes studied by Herrmann and co-workers at higher current no longer hold for certain exchange currents. For the simple kinetics, the distribution stays unimodal above a certain current (around 0.1). The qualitative trend remains true for the exchange current (a). Further, since exchange current (a) is symmetric with respect to $c = 0.5$, the phase behavior is also symmetric between lithiation and delithiation. However, the asymmetric exchange currents (b) and (c) induce an autocatalytic effect during delithiation and cause a larger degree of mosaic instability than lithiation while still suppressing the mosaic instability above a certain lithiation current. In fact, both (b) and (c) predict that the mosaic instability persists at large negative current.

Following Lim *et al.* [19], we define the uniformity coefficient $1 - \sigma_c/\sqrt{c(1-c)}$, which is 1 when $P(c = \langle c\rangle) = 1$ and 0 when σ_c is at its maximum, that is, $P(c = 0) = 1 - \langle c\rangle$ and $P(c = 1) = \langle c\rangle$. Figure 4 shows that the experimental exchange current (c) results in increasing uniformity with increasing total current and that, due to the skewed exchange current and reasons stated above, lithiation results in a more uniform distribution than delithiation. The result is in qualitative agreement with the experimental result from Lim *et al.* [19]. The theory overpredicts the uniformity for lithiation. This can be attributed to additional noise unaccounted for, such as particle size distribution and spatial inhomogeneity of the reaction kinetics. The asymmetry was also observed in another study by Li *et al.* [18], where the active particle fraction increases as a function of current and is higher for lithiation than for delithiation. This is consistent with the asymmetric exchange current since a smaller active particle fraction indicates a higher degree of heterogeneity and a lower uniformity coefficient.

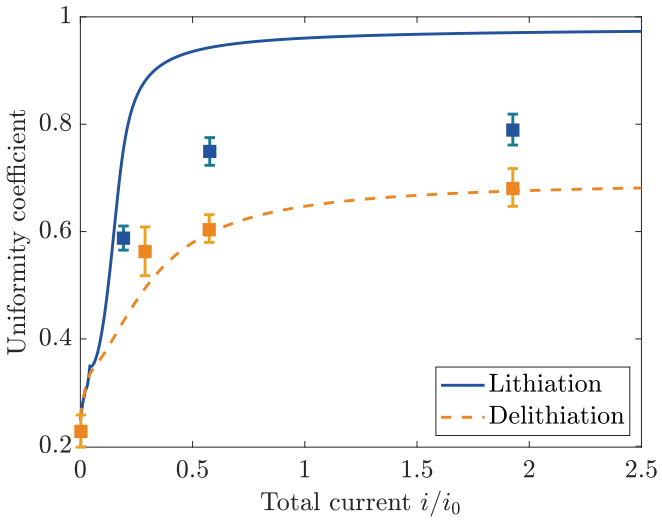

FIG. 4. Uniformity coefficient from the model (solid curves) and experiment [19] (squares with error bars). The model uses the experimental exchange current given in the same reference, $R_0 = 3(1-c)\sqrt{c(1-c)}$.

B. Driven phase separation at the critical point

In this section we present an example of a thermodynamically single-phase system that undergoes mosaic instability in certain reaction conditions. We choose the regular solution model with $\Omega = 2$ so that the system is at the critical point. As mentioned earlier, $\partial R/\partial c = -k_0\partial\mu/\partial c + (\mu_{\rm res} - \mu)\partial k/\partial c$. At the critical point c_0, $\mu'(c_0) = 0$ and $\partial R/\partial c(c_0) = [\mu_{\rm res} - \mu(c_0)]\partial k/\partial c(c_0)$; whether the reaction is autocatalytic or autoinhibitory is solely determined by the explicit dependence of the reaction rate on concentration $k(c)$ and the direction of the reaction.

For illustration purposes, we choose Butler-Volmer kinetics with the exchange current $R_0 = (1-c)^2 e^{\alpha\mu}$ [14]. In a lattice model, the exponent 2 indicates that the transition state excludes two empty sites [14]. The quadratic dependence on $1 - c$ enhances the autocatalysis and accelerates the backward reaction as c decreases. Figure 1 is a simulation with such thermodynamic and kinetic models, at $\mu_{\rm res} = -0.2$ and total reaction rate -0.1. It illustrates the diverging characteristics during the backward reaction.

Figure 5 shows the kinetic phase diagram of the system. Instability and a bimodal distribution occur at very low backward reaction rates. Unlike LFP, increasing the backward

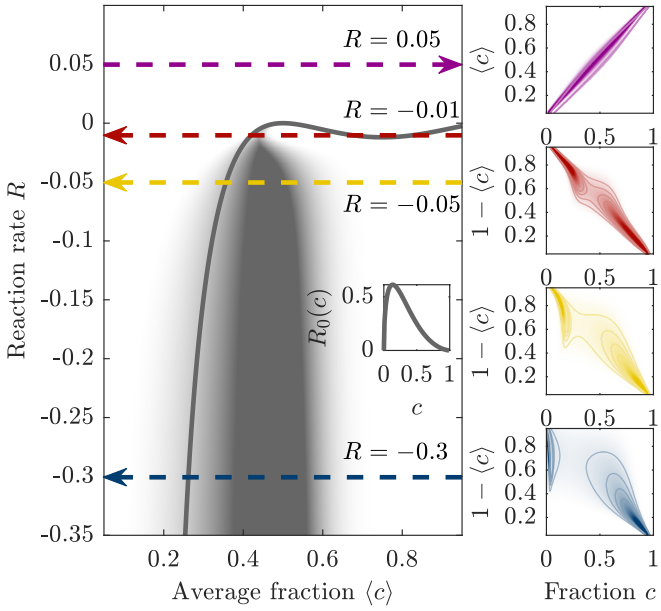

FIG. 5. Population dynamics applied to a system at the critical point ($\Omega = 2$ and $D_0 = \times 10^{-3}$). The exchange current is shown in the inset. The gray area is the region of mosaic instability. The colormap is the same as that of Fig. 3. The system is linearly unstable below the gray solid curve.

reaction rate leads to the expansion of the mosaic instability region. During the backward reaction, the distribution diverges so much that the population separates into two distinct "fictitious phases" while the forward reaction shows stable single-phase behavior. The region of mosaic instability is even more asymmetric than LFP with the asymmetric exchange current due to the second-order dependence on $1 - c$. The mosaic instability region is contained within the linearly unstable region, which is below the solid gray curve. We do not give the approximated mosaic instability region like the one above for LFP, because when the second peak in the PDF appears, the peak position is not always close to 0 or 1.

This leads to important applications in the interpretation of *in situ* and operando x-ray diffraction (XRD) experiments of electrodes, which measure the population density as a function of lattice parameters and thus the state of charge of the particles [58–61]. One should be cautious in deriving phases of a material from the XRD in a time-dependent experiment such as charge and discharge, as the XRD peaks may arise as a result of kinetic effects.

The mosaic instability defined for a particle ensemble can also inform us about the initiation of phase separation due to spinodal decomposition or nucleation within particles. In particular, the example presented here suggests that pattern formation may also arise when driven away from equilibrium through autocatalytic reactions even though the reactive mixture is thermodynamically stable. This could have implications in understanding and engineering phase separation in a variety of systems and patterns driven by electron transfer reactions. Negative differential resistance ($\partial R/\partial \Delta\mu < 0$) is not studied here in the context of population dynamics but can also lead to such fictitious phase separation.

IV. SUMMARY

We presented a theory of describing the equilibrium and dynamics of an ensemble of spatially homogeneous reactive particles that undergo reaction with the reservoir. The theory extends beyond the discrete particle simulation or the simplified reaction kinetics that was studied previously. Under the reaction-controlled condition, reaction kinetics determines the characteristics of the governing equation for the probability distribution of the particle ensemble. By introducing chemical fluctuation for any generalized reaction kinetics in a thermodynamically consistent way, the corresponding Fokker-Planck equation obeys detailed balance.

Through analytical approximation and numerical analysis of several model systems, we studied how reaction kinetics of the system affects the population dynamics and in some cases transforms the entire landscape of phase behavior for systems with the same thermodynamic properties. Suppression of phase separation or the induction thereof in single-phased systems has been observed. The analytical approximation for the boundary of mosaic instability based on the integral of the autocatalytic rate shows good agreement with numerical simulation. This reinforces our understanding that autocatalytic effects lie at the core of such phase separation behavior.

Therefore, knowledge of the reaction kinetics is crucial in understanding the dynamics of reaction-controlled systems. One can also envision engineering reactive surfaces to achieve desirable kinetic properties. The emergent phenomena observed here motivate us to further explore kinetically controlled phase separation in experiments using *in situ* analysis such as the aforementioned x-ray diffraction.

Although we did not address any possible spatial correlation or dependence in this paper, the theory can be extended to incorporate the external environment that the particles are subjected to by defining probability in the particle state space and physical space. For example, we can introduce other fields such as mass, temperature, and electric potential to consider transport phenomena, as well as the particle ensemble's interaction with the external fields. Particles in a porous medium can also be influenced by its highly localized environment. Any intrinsically variable property or such local variability that follows certain probability measures can also be incorporated in the theory. The population dynamics can also shed light on the spatially dependent behavior within the particles. For example, population dynamics offers a spatially agnostic statistical description of the concentration field such as its mean and variance for as long as it maintains isotropy and before patterns with sharp concentration gradient take over.

ACKNOWLEDGMENTS

This work was supported by Toyota Research Institute through the D3BATT Center on Data-Driven-Design of Rechargeable Batteries. The authors would like to thank D. Fraggedakis for useful discussions and E. Khoo and M. McEldrew for advice on the visualization and revising the manuscript.

[1] D. Ramkrishna, *Population Balances* (Academic, New York, 2000).
[2] D. Ramkrishna and M. R. Singh, Annu. Rev. Chem. Biomol. Eng. **5**, 123 (2014).
[3] I. Lifshitz and V. Slyozov, J. Phys. Chem. Solids **19**, 35 (1961).
[4] W. Dreyer, J. Jamnik, C. Guhlke, R. Huth, J. Moškon, and M. Gaberšček, Nat. Mater. **9**, 448 (2010).
[5] W. Dreyer, C. Guhlke, and R. Huth, Physica D **240**, 1008 (2011).
[6] A. Mielke and L. Truskinovsky, Arch. Ration. Mech. Anal. **203**, 577 (2012).
[7] F. Jafarpour, C. S. Wright, H. Gudjonson, J. Riebling, E. Dawson, K. Lo, A. Fiebig, S. Crosson, A. R. Dinner, and S. Iyer-Biswas, Phys. Rev. X **8**, 021007 (2018).
[8] C.-C. Shu, A. Chatterjee, G. Dunny, W.-S. Hu, and D. Ramkrishna, PLoS Comput. Biol. **7**, e1002140 (2011).
[9] A. Bonnefont, E. Savinova, and K. Krischer, Curr. Opin. Electrochem. **4**, 145 (2017).

[10] D. A. Crespo-Yapur, A. Bonnefont, R. Schuster, K. Krischer, and E. R. Savinova, Chem. Phys. Chem. **14**, 1117 (2013).

[11] D. A. Crespo-Yapur, A. Bonnefont, R. Schuster, K. Krischer, and E. R. Savinova, ChemElectroChem **1**, 1046 (2014).

[12] V. Johanek, M. Laurin, A. Grant, B. Kasemo, C. Henry, and J. Libuda, Science **304**, 1639 (2004).

[13] M. Z. Bazant, Faraday Discuss. **199**, 423 (2017).

[14] M. Z. Bazant, Acc. Chem. Res. **46**, 1144 (2013).

[15] W. Dreyer, C. Guhlke, and M. Herrmann, Continuum Mech. Therm. **23**, 211 (2011).

[16] W. Dreyer, R. Huth, A. Mielke, J. Rehberg, and M. Winkler, Z. Angew. Math. Phys. **66**, 293 (2015).

[17] C. Guhlke, P. Gajewski, M. Maurelli, P. K. Friz, and W. Dreyer, Continuum Mech. Therm. **30**, 593 (2018).

[18] Y. Li, F. El Gabaly, T. R. Ferguson, R. B. Smith, N. C. Bartelt, J. D. Sugar, K. R. Fenton, D. A. Cogswell, A. L. D. Kilcoyne, T. Tyliszczak, M. Z. Bazant, and W. C. Chueh, Nat. Mater. **13**, 1149 (2014).

[19] J. Lim, Y. Li, D. H. Alsem, H. So, S. C. Lee, P. Bai, D. A. Cogswell, X. Liu, N. Jin, Y. S. Yu, N. J. Salmon, D. A. Shapiro, M. Z. Bazant, T. Tyliszczak, and W. C. Chueh, Science **353**, 566 (2016).

[20] P. Bai and G. Tian, Electrochim. Acta **89**, 644 (2013).

[21] F. Schweitzer, *Browning Agents and Active Particles*, Springer Series in Synergetics (Springer, Berlin, 2007).

[22] G. R. Haynes and G. A. Voth, J. Chem. Phys. **103**, 10176 (1995).

[23] G. R. Haynes, G. A. Voth, and E. Pollak, Chem. Phys. Lett. **207**, 309 (1993).

[24] G. A. Voth, J. Chem. Phys. **97**, 5908 (1992).

[25] J. B. Straus, J. M. Gomez Llorente, and G. A. Voth, J. Chem. Phys. **98**, 4082 (1993).

[26] M. Schell, R. Kapral, and R. I. Cukier, J. Chem. Phys. **75**, 5879 (1981).

[27] E. Pollak and A. M. Berezhkovskii, J. Chem. Phys. **99**, 1344 (1993).

[28] M. Herrmann, B. Niethammer, and J. J. L. Velázquez, Multiscale Model. Simul. **10**, 818 (2012).

[29] M. Herrmann, B. Niethammer, and J. J. L. Velázquez, Arch. Ration. Mech. Anal. **214**, 803 (2014).

[30] T. D. Frank, *Nonlinear Fokker-Planck Equations*, Springer Series in Synergetics (Springer, Berlin, 2005).

[31] S. H. Strogatz, Physica D **143**, 1 (2000).

[32] R. E. Mirollo and S. H. Strogatz, SIAM J. Appl. Math. **50**, 1645 (1990).

[33] S. H. Strogatz, D. M. Abrams, A. McRobie, B. Eckhardt, and E. Ott, Nature (London) **438**, 43 (2005).

[34] D. Li, Y. Sun, Z. Yang, L. Gu, Y. Chen, and H. Zhou, Joule **2**, 1265 (2018).

[35] R. B. Smith and M. Z. Bazant, J. Electrochem. Soc. **164**, E3291 (2017).

[36] D. Burch and M. Z. Bazant, Nano Lett. **9**, 3795 (2009).

[37] T. R. Ferguson and M. Z. Bazant, Electrochim. Acta **146**, 89 (2014).

[38] T. R. Ferguson and M. Z. Bazant, J. Electrochem. Soc. **159**, A1967 (2012).

[39] N. C. Bartelt, Y. Li, J. D. Sugar, K. Fenton, A. L. D. Kilcoyne, D. A. Shapiro, T. Tyliszczak, W. C. Chueh, and F. E. Gabaly, Phys. Rev. Appl. **10**, 044056 (2018).

[40] D. Kondepudi and I. Prigogine, *Modern Thermodynamics* (Wiley, Chichester, 2014).

[41] P. Bai, D. A. Cogswell, and M. Z. Bazant, Nano Lett. **11**, 4890 (2011).

[42] D. A. Cogswell and M. Z. Bazant, ACS Nano **6**, 2215 (2012).

[43] D. A. Cogswell and M. Z. Bazant, Nano Lett. **13**, 3036 (2013).

[44] N. Nadkarni, E. Rejovitsky, D. Fraggedakis, C. V. Di Leo, R. B. Smith, P. Bai, and M. Z. Bazant, Phys. Rev. Mater. **2**, 085406 (2018).

[45] D. Chandler, *The Introduction to Modern Statistical Mechanics* (Oxford University Press, Oxford, 1987).

[46] H. Risken, *The Fokker-Planck Equation*, Springer Series in Synergetics Vol. 18 (Springer, Berlin, 1989).

[47] R. Jordan, D. Kinderlehrer, and F. Otto, SIAM J. Math. Anal. **29**, 1 (1998).

[48] K. Sekimoto, *Stochastic Energetics*, Lecture Notes in Physics Vol. 799 (Springer, Berlin, 2010).

[49] D. Reguera, J. M. Rubí, and J. M. G. Vilar, J. Phys. Chem. B **109**, 21502 (2005).

[50] R. Rao and M. Esposito, Phys. Rev. X **6**, 041064 (2016).

[51] U. Seifert, Phys. Rev. Lett. **95**, 040602 (2005).

[52] U. Seifert, Rep. Prog. Phys. **75**, 126001 (2012).

[53] C. Van den Broeck and M. Esposito, Phys. Rev. E **82**, 011144 (2010).

[54] D. T. Gillespie, J. Chem. Phys. **113**, 297 (2000).

[55] D. T. Gillespie, Annu. Rev. Phys. Chem. **58**, 35 (2007).

[56] A. Ceccato and D. Frezzato, J. Chem. Phys. **148**, 064114 (2018).

[57] J. Newman and K. E. Thomas-Alyea, *Electrochemical Systems* (Wiley, New York, 2012).

[58] Y.-N. Zhou, J.-L. Yue, E. Hu, H. Li, L. Gu, K.-W. Nam, S.-M. Bak, X. Yu, J. Liu, J. Bai, E. Dooryhee, Z.-W. Fu, and X.-Q. Yang, Adv. Energy Mater. **6**, 1600597 (2016).

[59] H. Liu, F. C. Strobridge, O. J. Borkiewicz, K. M. Wiaderek, K. W. Chapman, P. J. Chupas, and C. P. Grey, Science **344**, 1252817 (2014).

[60] A. Singer, A. Ulvestad, H.-M. Cho, J. W. Kim, J. Maser, R. Harder, Y. S. Meng, and O. G. Shpyrko, Nano Lett. **14**, 5295 (2014).

[61] J. Hong, H. Zhao, J. Jungjin, K. Lim, K. Lim, W. E. Gent, J. Weker, R. D. Braatz, M. F. Toney, M. Z. Bazant, and W. C. Chueh (unpublished).